Journal of Zhejiang University-SCIENCE A (Applied Physics & Engineering)
ISSN 1673-565X (Print); ISSN 1862-1775 (Online)
www.jzus.zju.edu.cn; www.springerlink.com
E-mail: jzus@zju.edu.cn

Effects of mounting positions and boundary conditions on the sound transmission loss of panels in a niche*

Dan YAO[1], Jie ZHANG[1,2], Rui-qian WANG[1,3], Xin-biao XIAO[†‡1]

[1]*State Key Laboratory of Traction Power, Southwest Jiaotong University, Chengdu 610031, China*

[2]*State Key Laboratory of Polymer Materials Engineering/Polymer Research Institute, Sichuan University, Chengdu 610065, China*

[3]*School of Urban Rail Transit, Changzhou University, Changzhou 213164, China*

[†]E-mail: xiao@home.swjtu.edu.cn

Received Sept. 24, 2019; Revision accepted Dec. 24, 2019; Crosschecked Jan. 7, 2020

Abstract: The sound insulation performance of railway car body structures is critical for the control of rail vehicle interior noise. In sound transmission loss (STL) measurements, a niche with a large depth is necessary to allow for mounting the wide range of thicknesses of railway car body panels and for the mechanical isolation of the two rooms. In this study, two typical interior floor panels are tested in a series of mounting conditions and mechanical boundary conditions. The change of STL results during measurement is also predicted by an STL prediction model based on the finite element method. At lower frequencies, the STL results are influenced by both the mounting positions and the mechanical boundary conditions. At higher frequencies, the STL results are mainly influenced by the mechanical boundary conditions. Differences between the panel in the infinite baffle and niches at the resonance and off-resonance frequencies are different. Considering both the effects of mounting positions and mechanical boundary conditions, the existence of the cavity amplifies the STL difference caused by the mechanical boundary conditions.

Key words: Sound transmission loss (STL); Railway interior floor; Boundary condition; Mounting position; Niche effect
https://doi.org/10.1631/jzus.A1900494 **CLC number:** TU112.21

1 Introduction

With the development of railway vehicles, the noise problem inside railway vehicles has increasingly attracted attention (Thompson, 2009; Jin, 2014). The vibro-acoustic characteristics of the panels of rail vehicles directly affect interior noise. Therefore, it is necessary to improve the sound transmission loss (STL) of the panels (Eade and Hardy, 1977; Zhang et al., 2016).

The STL of panels can be evaluated in the laboratory using the sound pressure method (ISO, 2010a, 2010b, 2010c, 2010d) and the sound intensity method (ISO, 2000, 2002). The ISO standard specified some factors since STL results of building elements differ by the change of design of laboratories and mounting conditions. For large specimens such as walls, the area of the test opening should be approximately 10 m^2, and between 10 m^2 and 20 m^2 for floors (ISO, 2010d). For small-sized test specimens such as windows and glazing, the preferred dimensions of the test opening are 1.25 m×1.50 m, and the test opening has a maximum depth of 500 mm, with staggered niches; the niches on both sides of the windows shall have different depths, preferably at a ratio of about 2:1 (ISO, 2010b).

At present, in railway panel STL measurement, small-sized test elements (Xie et al., 2006; Kim and

‡ Corresponding author

* Project supported by the National Key Research and Development Program of China (No. 2016YFE0205200) and the National Natural Science Foundation of China (No. U1834201)

ORCID: Dan YAO, https://orcid.org/0000-0003-2793-2687; Xin-biao XIAO, https://orcid.org/0000-0001-5078-4817

Kim, 2011; Kim K et al., 2012; Liu et al., 2014; Kim H et al., 2016; Dai et al., 2019) are generally used to guide the test process for reduced cost. Furthermore, railway vehicle components of different sizes are adapted to fit in the test opening. For railway panel structures, there is no specific standard for STL measurement, and only the STL measurement standards for building elements can be referred to. However, it is not very easy for railway panel structures to meet all the test specifications of the standards for building elements.

In order to test railway panel structures in different components with a wide range of thicknesses up to a maximum of 100 mm, the depth of the sound transmission loss niche must be large. The wall between the source and the receiving room in the laboratory is necessarily heavy and thick to avoid flanking transmission. A niche with a large depth is necessary to allow for mounting the wide range of thicknesses of railway car body panels and for the mechanical isolation of the two rooms. Then, the depth of the test opening may exceed 500 mm. With staggered niches, the mounting positions become limited, and the test element may not meet the requirement that the niches on both sides shall have different depths, preferably in a ratio of about 2:1. The mechanical boundary conditions (simplified as boundary conditions in the remainder of this paper) also change with the mounting positions. The smaller the test element, the more sensitive the results will be to edge constraint conditions and the mounting positions (ISO, 2010b). Therefore, the test results will be significantly influenced by different mounting positions and boundary conditions.

The 'niche effect' (Sgard et al., 2015) is apparent at frequencies below the coincidence frequency. The STL of a single panel in niches is smaller than in an infinite rigid baffle, and the maximum difference occurs when the panel is placed at the centre of the niche (Kim et al., 2004; Vinokur, 2006; Gholami, 2013; Sgard et al., 2013). The main reason for this is that the structural modes of the panel are strongly coupled with the acoustic modes at both sides of the niche (Dijckmans and Vermeir, 2012). The influence of boundary conditions on STL results has been discussed by some researchers (Utley and Fletcher, 1969, 1973; Kihlman and Nilsson, 1972). Comparisons of STL difference on single glass (Utley and Fletcher, 1969) and double glazing (Utley and Fletcher, 1973) in different window mounting frames have been carried out, for different mounting boundary conditions, where the difference in the STL results can reach 10 dB. For small-sized panels, the STL is dependent on boundary conditions at frequencies below coincidence. The boundary conditions around the panel are usually defined as simply supported, free, or clamped in numerical methods (Xin and Lu, 2009).

Both the mounting positions and the boundary conditions have essential effects on the STL results of the panel and cannot be neglected in the STL measurement in the laboratory. The evaluation of the effects can provide a reference for a better experimental design and is also helpful in interpreting test results with realistic structures. However, few studies have considered both the effects of mounting positions and boundary conditions. Further research is needed to identify the significant frequency bands of the two influencing factors, and which factor has a more significant impact.

In this study, the influence of the mounting position and boundary conditions of lightweight panels in railway vehicles in an STL test niche is investigated. The differences in STL caused by the mounting conditions and the boundary conditions are explained by test and prediction. Then, the test method, test facility, and specimens under test are introduced. Test results of two typical railway interior floor panels at three mounting positions with two typical boundary conditions are shown. Next, the prediction model based on the finite element method is introduced and validated with test results. At last, using the prediction model, the influence of the mounting positions and the boundary conditions on STL is first investigated separately and then the two effects are both considered simultaneously.

2 STL measurements

2.1 Test method

The experimental set-up for measuring the STL consists of a source room, a receiving room, and a panel placed in the wall. Assuming a perfectly diffuse sound field in the source room and the receiving room, the STL is calculated as follows (ISO, 2010b):

$$\mathrm{STL}=L_1-L_2+10\lg\frac{S}{A}, \tag{1}$$

where L_1 and L_2 are the averaged sound pressure levels in the source room and the receiving room (dB), respectively. S is the area of the test opening (m^2). A is calculated from the reverberation time using Sabine's formula as follows:

$$A=\frac{0.16V}{T}, \tag{2}$$

where V is the receiving room volume (m^3), and T is the reverberation time (s).

2.2 Test facility

Fig. 1 shows the source room and receiving room in the present study. The dimensions of the two rooms meet the requirement that the volumes of the rooms shall be at least 50 m^3 (ISO, 2010d): the source room is approximately 5.4 m×4.1 m×3.3 m, and the receiving room is approximately 4.5 m×4.1 m×3.3 m. The reverberation time in the two rooms is within the range of $1\leq T\leq 2(V/50)^{2/3}$ in 1/3 octave bands centred from 100 to 3150 Hz (ISO, 2010d), as shown in Fig. 2.

To eliminate the influence of the microphone positions, six spatial, randomly distributed microphones are used in the two rooms. The separation distances for microphone positions meet the requirement in ISO 10140-4 (ISO, 2010c): the distance between the microphones (or the distance between the microphone and the room boundaries) is larger than 0.7 m, and the distance between the microphone and the test element (or the sound source) is larger than 1.0 m. An omnidirectional loudspeaker is placed in six positions (four regular positions and two corner positions) during the test to eliminate the influence of the sound source. The number of loudspeaker positions is qualified according to the procedure in annexe D of ISO 10140-5 (ISO, 2010d). The sound pressure levels are averaged according to energy level based on the results for six spatial randomly distributed microphones. The averaged sound pressure level is calculated by

$$P=10\lg\frac{1}{n}\sum_{j=1}^{n}10^{P_j/10}, \tag{3}$$

where P_1, P_2, …, P_n are sound pressure levels at n different positions in the room.

During the measurement of reverberation time, the omnidirectional loudspeaker is placed in six positions (three regular positions and three corner positions) to eliminate the influence of the sound source. The reverberation time is linearly averaged based on the results for six spatial randomly distributed microphones and the results for loudspeaker at six different positions.

The STL of each loudspeaker position is determined using Eq. (1). The averaged STL of six loudspeaker positions is calculated by

$$R=-10\lg\frac{1}{n}\sum_{i=1}^{n}10^{-R_i/10}, \tag{4}$$

where R is the averaged STL of n loudspeaker positions, and R_i is the STL of the ith loudspeaker position.

The wall between the source room and the receiving room is filled with a sandwich structure with a surface density of approximately 75 kg/m^2. The maximum measurable weighted sound reduction index, R_w, of the test facility is 65 dB. The minimum difference of STL between the filler wall and the test elements (the aluminium panel and the aluminium honeycomb panel tested in this study) is 17.5 dB in the 1/3 octave band centred from 100 to 3150 Hz (the difference is a direct comparison between the filler wall and the test elements; since the surface area of the filler wall is about 10 times the area of the test elements, the actual difference is even larger). The difference is larger than 15 dB as required in ISO 10140-2 (ISO, 2010b). The aperture between the two rooms has dimensions of about 0.985 m×0.970 m×0.560 m. There is an iron frame in the STL test niche to ensure that the test element is fixed, mainly when the size of the panel is slightly smaller than the niche. The distance between the source room and the iron frame is approximately 175 mm. Thus, the mounting positions are limited. The panel is fixed with eight screw bolts on the side closer to the source room and four wooden blocks at the four corners on the side closer to the receiving room, as shown in Fig. 3. The lengths of the screw bolts and wooden blocks vary with the mounting position of the panel. The front and rear boundaries of the test panel are sealed with the putty to prevent sound leakage.

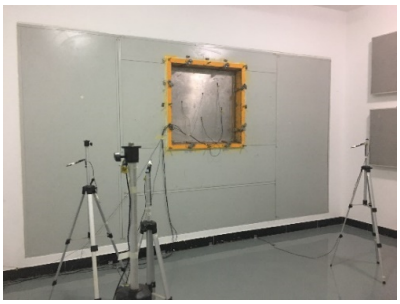

(a)

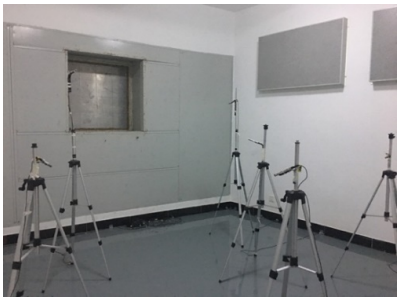

(b)

Fig. 1 Rooms for the STL measurements
(a) Source room; (b) Receiving room

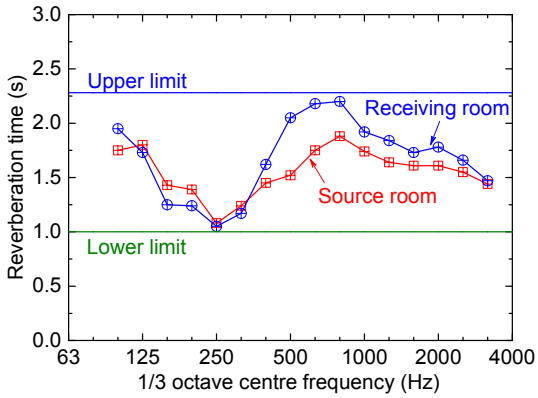

Fig. 2 Reverberation times of the two rooms

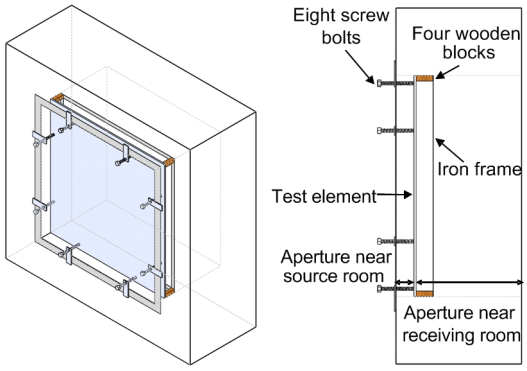

Fig. 3 Installation boundary conditions of the panel

2.3 Specimens under test

Typical railway interior floor panels (an aluminium panel and an aluminium honeycomb panel) are measured in this study. The surface area of the two panels is 0.985 m×0.970 m. The thicknesses of the aluminium panel and the aluminium honeycomb panel are 10 mm and 18 mm, and their surface mass densities are 27.0 kg/m^2 and 8.16 kg/m^2, respectively.

When the test panel is placed in the wall with an aperture, different mounting positions result in different STL results, and the boundary conditions around the panel will be differently restricted by the test facility. To investigate the influence of the mounting positions and boundary conditions on the STL of the panels, three conditions contain two boundary conditions and three mounting positions are summarised in Table 1. The thickness of the panel (h), the depth of the aperture near the source room (T_s), and the depth of the aperture near the receiving room (T_r) for the three conditions are also shown in Table 1.

For Conditions 1 and 2, the restraints on the side of the source room are eight screw bolts, while the restraints on the side of the receiving room are four wooden blocks. For Condition 3, the mounting position is close to the iron frame, the restraints on the side of the source room are eight screw bolts, while the restraint on the side of the receiving room becomes the whole iron frame.

3 Measurement results

3.1 STL results for the aluminium panel

The STL result is calculated in two parts: the sound pressure level difference between the source room and the receiving room (L_1−L_2), and the correction results based on the reverberation time ($10\lg\frac{ST}{0.16V}$). The influence of microphone positions and source positions on the two parts is first considered, and then the repeatability uncertainty on STL is calculated with the combination of the two intermediate results.

The influence of microphone positions and source positions on sound pressure level differences is first considered. The repeatability for Condition 3 of the aluminium panel is taken as an example. The standard deviations for six microphone positions of

Table 1 STL test conditions for the aluminium and the aluminium honeycomb panels

Test panel	Test condition	Mounting position			Boundary condition	
		T_s (mm)	h (mm)	T_r (mm)	Restraints on the source room side	Restraints on the receiving room side
Aluminium panel	Condition 1	0	10	550	8 screw bolts	4 wooden blocks
	Condition 2	80	10	470	8 screw bolts	4 wooden blocks
	Condition 3	165	10	385	8 screw bolts	Iron frame
Aluminium honeycomb panel	Condition 1	0	18	542	8 screw bolts	4 wooden blocks
	Condition 2	75	18	467	8 screw bolts	4 wooden blocks
	Condition 3	157	18	385	8 screw bolts	Iron frame

the sound pressure level in source and receiving rooms at one source position is shown in Fig. 4a. The standard deviation for six source positions of L_1−L_2 is shown in Fig. 4b.

It can be seen that the standard deviation for six microphone positions of sound pressure level is smaller than 1 dB in the 1/3 octave bands centred from 630 to 3150 Hz, whether in the source room or the receiving room. However, the sound pressure levels are different in the 1/3 octave bands centred from 100 to 500 Hz. The differences are due to the lack of totally reverberant conditions at low frequencies in the two rooms. The sound field approximates a diffuse field above the Schroeder frequency (Schroeder, 1996), and the Schroeder frequency is calculated by

$$f_s = 2000\sqrt{\frac{T}{V_r}}, \tag{5}$$

where V_r is the room volume (m^3).

The Schroeder frequency of the source room is approximately 400 Hz and 500 Hz for the receiving room in the 1/3 octave band. Therefore, the difference in sound pressure level among the six microphones is small in the 1/3 octave bands centred from 630 to 3150 Hz. The reverberation time results, as shown in Fig. 2, are used to calculate the Schroeder frequency.

The standard deviation for six source positions of L_1−L_2 is smaller than 2 dB in the 1/3 octave bands centred from 100 to 3150 Hz. At lower frequencies (i.e. the 1/3 octave bands centred from 100 to 500 Hz), the effect of microphone position on the test results can be reduced with the averaged sound pressure levels. The effect of sound source position on the test results can be reduced with the averaged STL.

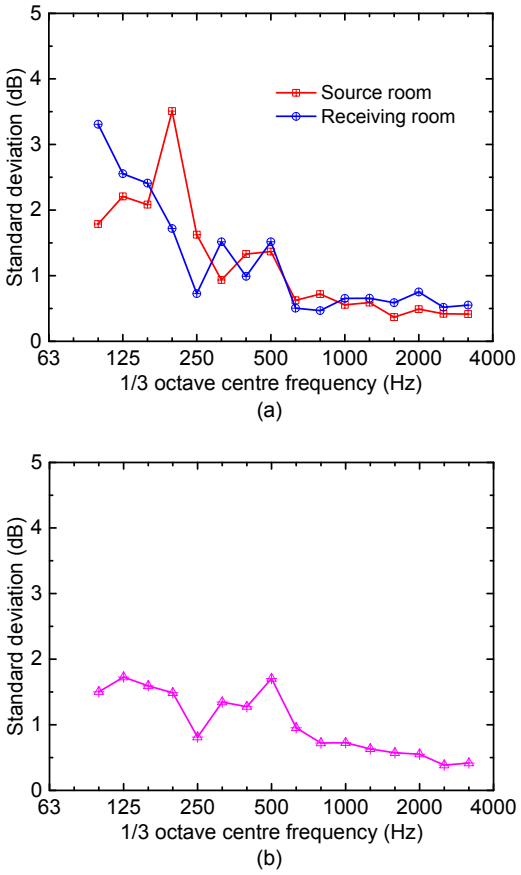

Fig. 4 Influence of microphone positions and source positions on sound pressure level differences
(a) Standard deviation for six microphone positions of sound pressure level in source and receiving rooms at one source position; (b) Standard deviation for six source positions of L_1−L_2

Then, the correction results based on the reverberation time in the receiving room are measured. The influence of microphone positions and source positions is considered. The repeatability for Condition 3 of the aluminium panel is taken as an example. The

standard deviation for six microphone positions of the correction results based on the reverberation time at one source position is shown in Fig. 5a. The standard deviation for six source positions of the correction results based on the reverberation time is shown in Fig. 5b, the reverberation time is linearly averaged based on the results for six spatial randomly distributed microphones.

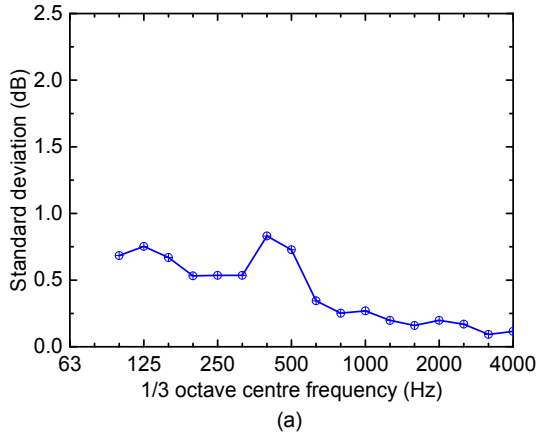

Fig. 5 Influence of microphone positions and source positions on the correction results based on the reverberation time

(a) Standard deviation for six microphone positions at one source position; (b) Standard deviation for six source positions

It can be seen that the standard deviation for six microphone positions of the correction results based on the reverberation time is smaller than 1 dB in the 1/3 octave bands centred from 100 to 3150 Hz. The standard deviation for six source positions is also smaller than 1 dB in the 1/3 octave bands centred from 100 to 3150 Hz. The difference in correction results based on the reverberation time is obviously smaller than the difference in the sound pressure level difference in Fig. 4.

Finally, the repeatability uncertainty on STL is calculated with the combination of the two uncertainties, L_1–L_2 and $10\lg\frac{ST}{0.16V}$, with the positive square root of a sum of the two uncertainties (ISO, 2014). The repeatability uncertainty results for the three conditions of the aluminium panel are shown in Fig. 6. The results are also compared with the maximum standard deviation of repeatability of inter-laboratory tests in ISO 12999-1 (ISO, 2014). The repeatability uncertainties on STL for the aluminium panel for the three conditions are smaller than the maximum standard deviation in ISO 12999-1 in most 1/3 octave bands centred from 100 to 3150 Hz.

The STL test results for the three conditions are shown in Fig. 7. The standard deviations for the three conditions are also given. The mass law transmission loss (Cremer, 1942) for random incidence and the critical frequency (f_c) of the panels are shown for interpretation.

Considering the standard deviation larger than 1.0 dB, the variation in the lower frequencies (i.e. the 1/3 octave bands centred from 100 to 250 Hz for the aluminium panel) indicates that the STL decreases as T_s increases from 0 to 165 mm. The variation in the higher frequencies (i.e. the 1/3 octave bands centred at 800 Hz for the aluminium panel) indicates that the STL is the greatest when T_s is 165 mm, the smallest when T_s is 80 mm, and intermediate when T_s is 0 mm. At frequencies below the critical frequency, the STL differences in 1/3 octave bands centred from 315

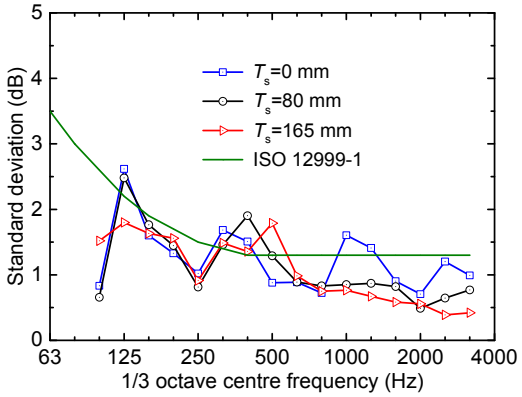

Fig. 6 Repeatability uncertainties on STL for the aluminium panel for Conditions 1–3

to 630 Hz and 1000 to 1250 Hz are not very large. This may be due to the influence of repeatability uncertainty. The standard deviations of the three conditions are only larger than the repeatability uncertainty on STL for Conditions 1−3 in 1/3 octave bands centred at 100, 250, 800, and 1600 Hz.

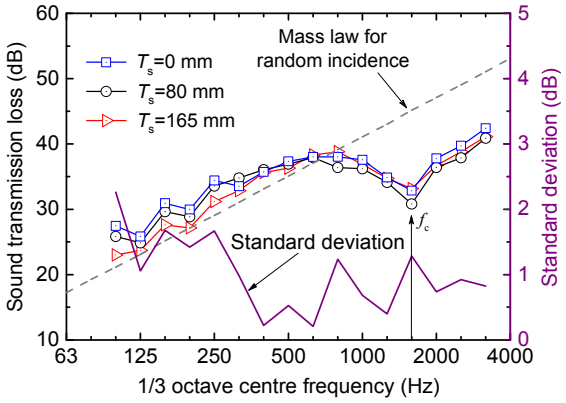

Fig. 7 STL test results for the aluminium panel for Conditions 1–3

3.2 STL results for the aluminium honeycomb panel

The repeatability uncertainties on STL for the three conditions of the aluminium honeycomb panel are shown in Fig. 8. The STL test results for the aluminium honeycomb panel for the three conditions are shown in Fig. 9.

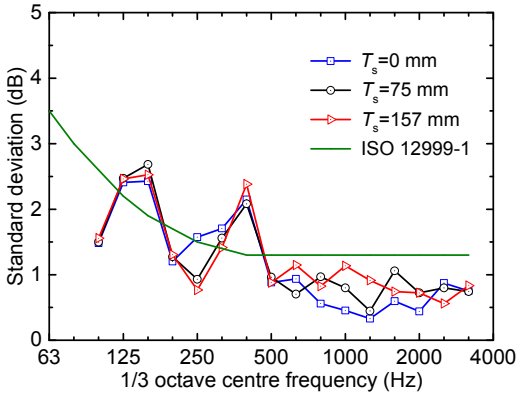

Fig. 8 Repeatability uncertainties on STL for the aluminium honeycomb panel for Conditions 1–3

The repeatability uncertainties on STL for the aluminium honeycomb panel for the three conditions are smaller than the maximum standard deviation in ISO 12999-1 in most 1/3 octave bands centred from 100 to 3150 Hz.

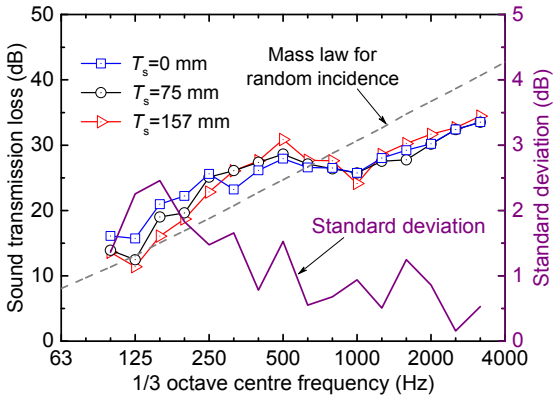

Fig. 9 STL test results for the aluminium honeycomb panel for Conditions 1–3

Considering the standard deviation larger than 1.0 dB, the variation in the lower frequencies (i.e. the 1/3 octave bands centred from 100 to 250 Hz for the aluminium honeycomb panel) indicates that the STL decreases as T_s increases from 0 to 157 mm. The variation at the higher frequencies (i.e. the 1/3 octave bands centred at 500 Hz for the aluminium honeycomb panel) indicates that the STL increases as T_s increases from 0 to 157 mm. At frequencies below the STL dip at 1000 Hz, the STL difference in 1/3 octave bands centred at 400, 630, and 800 Hz is not very large. This may be due to the influence of repeatability uncertainty. The standard deviations of the three conditions are larger than the repeatability uncertainty on STL for Conditions 1–3 in 1/3 octave bands centred at 200, 500, and 1600 Hz.

During the STL measurements, the STL results can be influenced by the repeatability uncertainty components, such as the microphone positions and source positions. The STL results can also be influenced by the uncertainties due to differences in mounting positions and boundary conditions. In each measurement setup, the positions of sound source and microphones are nearly the same, so the uncertainty due to microphone and source positions can be eliminated. Summarising the variation of the two panels for three conditions, it is found that the STL results decrease when T_s increases from 0 to 165 mm (or 157 mm) at lower frequencies, but at the higher

frequencies, the STL results become larger when the panel is in Condition 3 compared with Conditions 1 and 2. Since it is not very easy to ensure that the test results are only affected by a single variable, an STL prediction model has been established based on the finite element method to investigate the influence of the mounting positions and boundary conditions. The influence of the microphone positions and source positions is not considered in the prediction model.

4 STL predictions

4.1 Prediction model and validation

The STL prediction model based on the finite element method is established in LMS Virtual. Lab. The transmission loss model system consists of a panel inside an aperture separating two rooms (Schaffer and Pucher, 2013), as shown in Fig. 10.

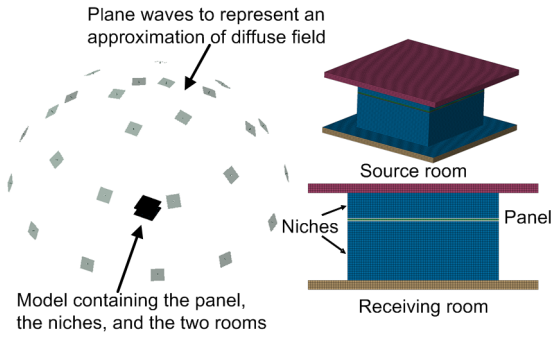

Fig. 10 STL prediction model

The source room and the receiving room are both represented by semi-infinite fluids; the automatically matched layer (AML) condition is used to represent a non-reflecting boundary condition in the source room and the receiving room, and the condition allows consideration of narrow meshing at both sides. The niches and the panel are represented by 3D solid elements. The depth of the niche and the thickness of the panel can be simulated by changing the solid element of the niches and the panel. The material properties of the niches are set as air; the material properties of the panel are adjusted according to the actual situation.

A set of uncorrelated plane waves is used to represent an approximation of a diffuse field. For each load condition, the incident power W_{I} is directly deduced from the given amplitude of the incident waves, which can be defined as

$$W_{\mathrm{I}}=\frac{|P_i|^2}{2\rho_0 c_0}L_{\mathrm{a}}L_{\mathrm{b}}\cos\varphi_i, \tag{6}$$

where P_i is the acoustic pressure amplitude; L_{a} and L_{b} are the length and width of the panel, respectively; φ_i is the incident angle; ρ_0 and c_0 are the density and sound speed of the air, respectively.

The sound power radiated directly by the panel in the receiving room, W_{T} (Fuller et al., 1996), is defined as

$$W_{\mathrm{T}}=\int_S\frac{1}{2}\mathrm{Re}\left\{\tilde{p}(r)\tilde{v}^*(r)\right\}\mathrm{d}S, \tag{7}$$

where $\tilde{p}(r)$ is the total complex acoustic pressure in the AML surface, and $\tilde{v}^*(r)$ is the normal surface velocity amplitude of the AML surface.

The STL is analysed independently under different load conditions; the total incident power and radiated power are obtained by linear summation of the different load conditions (Mao and Pietrzko, 2013).

The mounting position is modelled by the change of the front and rear cavities. The boundary conditions of the panel can be set as free, simply supported, clamped or other complex boundary conditions. When the boundary conditions of the aluminium panel are set as free, the degrees of freedom around the panel are non-constrained in all directions. When the boundary conditions of the aluminium panel are set as simply supported, the degrees of freedom around the panel are constrained in the direction vertical to the panel. When the boundary conditions of the aluminium panel are set as clamped, the degrees of freedom around the panel are constrained in all directions. For complex boundary conditions, the boundary conditions of the prediction model are basically similar to the actual test boundary conditions: the degrees of freedom of the elements corresponding with constrained areas are fixed. The simulations of two boundary conditions in Table 1, named ‘8 screw bolts, 4 wooden blocks’ and ‘8 screw bolts, iron frame’, are shown in Fig. 11. The degrees of freedom of the elements corresponding with the

screw bolts, the wooden blocks, and the iron frame are constrained in the direction vertical to the panel.

The aluminium panel is taken as an example to investigate the effect of front and rear cavities, the mounting positions, and the boundary conditions. The density of the fluid, speed inside the fluid, mechanical properties of the aluminium panel, and dimensions of the niche and the panel are detailed in Table 2.

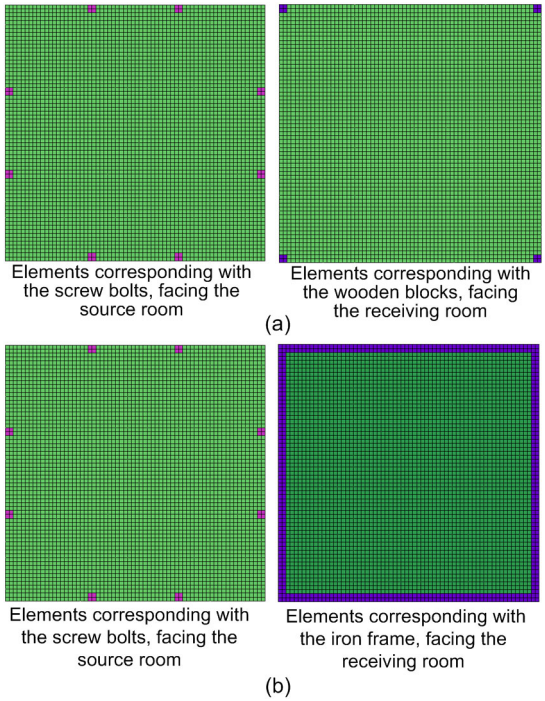

Fig. 11 Simulations of two boundary conditions
(a) 8 screw bolts, 4 wooden blocks; (b) 8 screw bolts, iron frame

Table 2 Values of model parameters

Parameter	Value
Density of fluid, ρ_0 (kg/m^3)	1.213
Speed inside fluid, c_0 (m/s)	342.2
Young's modulus of the panel, E (GPa)	71
Poisson's ratio of the panel, v	0.33
Damping loss factor of the panel, η	0.002
Density of the panel, ρ_s (kg/m^3)	2700
Lateral dimension, x (m)	0.985
Longitudinal dimension, y (m)	0.970
Thickness of the tunnel, d (m)	0.56
Thickness of the panel, h (m)	0.01

The element size of the acoustic mesh (the two rooms and the niches) is 15 mm, with six elements per wavelength for accurately modelling acoustic wave propagation, and the maximum frequency is 3802 Hz. Since the AML surface can be considered as a very limited mesh, the two rooms are represented with four layers of elements, used in relation to the intended accuracy and computational efficiency (de Langhe et al., 2016).

The STL results are calculated at discrete frequencies (referred to the 1/60 octave band frequencies), and results in the 1/3 octave band are obtained by summing the radiated power and incident power over each 1/3 octave band first, and then the ratio of the results is taken. Since the number of incident plane waves may influence the calculated STL, the convergence of the STL solution for the panel is checked, as shown in Fig. 12.

For this STL prediction model, too few plane waves will cause an overestimate of STL results at high frequencies. Three plane waves and 12 plane waves are not sufficient for a good diffuse field performance. Finally, 25 equally divided directions of incident plane waves are used to represent an approximation of a diffuse field considering the computational efficiency. The comparisons of the measured and predicted results for Conditions 1–3 of the aluminium panel are shown in Fig. 13.

As can be seen from Fig. 13, the tendency of STL results during the measurement can be completely simulated by the prediction model. The STL results decrease when T_s increases from 0 to 165 mm at lower frequencies; at higher frequencies, the STL results for Condition 3 are the largest, because of the influence of boundary conditions. STL results are affected by both the niches and the boundary conditions; the impact of boundary conditions is larger at higher frequencies. The reason for this is given in detail in Section 5.3.1.

However, the current model may not adequately simulate the actual test environment. The test rooms are two reverberation rooms with finite volume, but in the prediction model, the two rooms are semi-infinite, with a reverberation room and an anechoic room. This may affect the STL results. Further improvements are needed to simulate the actual environmental model.

The STL prediction model has also been validated with the STL results of a panel inside a niche in (Sgard et al., 2013, 2015). The STL results in those references have been successfully compared with

experimental data. The STL results of an 8-mm thick aluminium panel placed at the centre of a niche have been calculated with the prediction model in this study. The element size, and the dimensions of the panel and the niche are exactly the same as those in the references. The STL results are calculated at discrete frequencies from 100 to 1500 Hz, and the step size is 2 Hz. Fig. 14 shows that there is excellent agreement between the prediction model and the numerical approach in (Sgard et al., 2013, 2015).

In general, it is feasible to use this model to calculate the STL values of the panel structure to compare the STL for different mounting positions and boundary conditions.

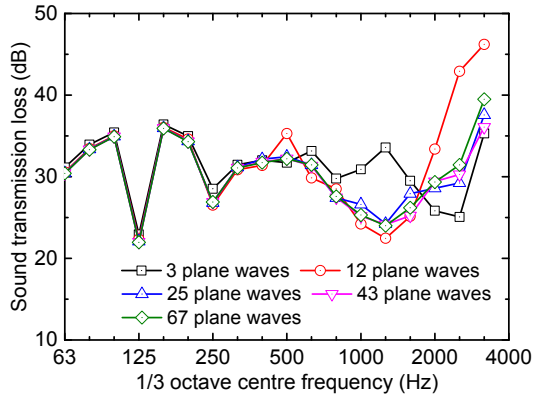

Fig. 12 Influence of the number of incident plane waves on STL results

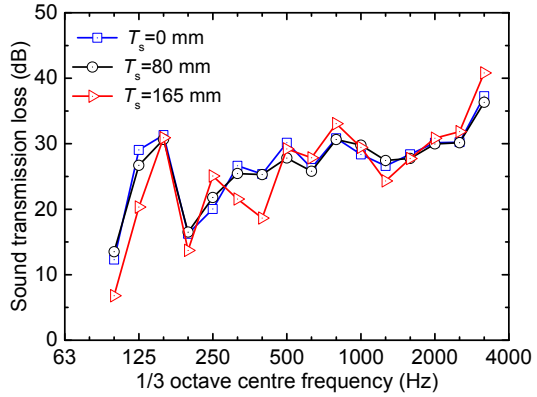

Fig. 13 STL predicted results for three conditions

4.2 Prediction conditions

In order to investigate the influences of the front and rear cavities, the mounting positions, and the boundary conditions separately, prediction conditions containing different mounting positions and boundary conditions are summarised in Table 3. The mounting position is modelled by the change of the front and rear cavities. The different boundary conditions are modelled by changing the degrees of freedom of the panel boundary.

The effect of front and rear cavities on the STL results can be obtained by comparing the STL results of Conditions 1–4. Condition 1 represents the panel in an infinite baffle; for Conditions 2 and 3, there only exists one side of the aperture; Condition 4 represents the panel in niches when T_s=165 mm, T_r=385 mm.

The effect of mounting positions can be obtained by the results of Conditions 4–6, which are under the same boundary conditions.

The effect of boundary conditions can be obtained by the results of those under the same mounting positions. The impact of the niche effect on the boundary conditions is also considered. Conditions 1 and 7–10 represent five boundary conditions when the panel is in an infinite baffle, while Conditions 4 and 11–14 represent five boundary conditions when the panel is in niches.

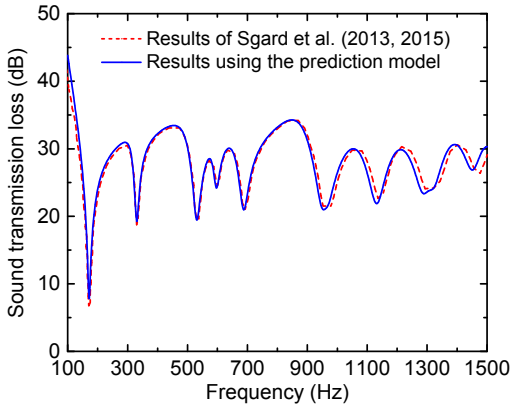

Fig. 14 Comparison of predicted STL results and results of Sgard et al. (2013, 2015)

5 Results and discussion

5.1 Effects of the front and rear cavities

To analyse the effect of front and rear cavities on the STL results, the STL results for an aluminium panel in an infinite baffle and niches are predicted, and the boundary conditions are simply supported. The STL difference results between the panel in the

infinite baffle and niches for the three conditions are shown in Fig. 15.

Table 3 STL prediction conditions for the aluminium panel

Prediction condition	Mounting position			Boundary condition
	T_s (mm)	h (mm)	T_r (mm)	
Condition 1	0	10	0	Simply support
Condition 2	165	10	0	Simply support
Condition 3	0	10	385	Simply support
Condition 4	165	10	385	Simply support
Condition 5	0	10	550	Simply support
Condition 6	80	10	470	Simply support
Condition 7	0	10	0	8 screw bolts, 4 wooden blocks
Condition 8	0	10	0	8 screw bolts, iron frame
Condition 9	0	10	0	Free
Condition 10	0	10	0	Clamped
Condition 11	165	10	385	8 screw bolts, 4 wooden blocks
Condition 12	165	10	385	8 screw bolts, iron frame
Condition 13	165	10	385	Free
Condition 14	165	10	385	Clamped

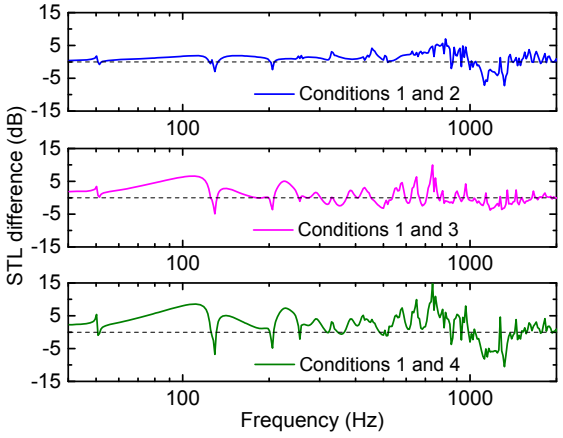

Fig. 15 Predicted STL difference results between the panel in the infinite baffle and niches

The STL of the panel in niches is smaller than in an infinite rigid baffle at most frequencies from 40 to 2000 Hz. The maximum difference occurs when the panel is in niches with the front and rear cavities, compared to the difference when only one side of the cavity is present. The difference at the off-resonance frequencies is generally greater than 0, while the difference at resonance frequencies and the critical frequency is generally less than 0.

Two typical resonance frequencies (129 and 205 Hz) and two typical off-resonance frequencies (109 and 228 Hz) with significant STL differences are selected, and the reasons for the differences are explained by the sound pressure level colour map, as shown in Figs. 16 and 17.

The STL results are influenced by the existence of the cavities on two sides. As can be seen from Fig. 16, the sound pressure level colour map for Conditions 1 and 3 are precisely the same, and so are those for Conditions 2 and 4. The aperture on the side of the source room amplifies the sound pressure at the four frequencies. For the sound pressure level of the AML surface of the receiving room, as shown in Fig. 17, the sound pressure level colour map for Conditions 1 and 2 are basically the same, and so are those for Conditions 3 and 4, but the sound pressure levels for resonance frequencies and off-resonance frequencies are different. For off-resonance frequencies, the acoustic cavity at the receiving side causes an increase of the sound pressure in the receiving room, and the increase becomes more significant when the panel is in niches with the front and rear cavities, compared to the increase when only the receiver side of the cavity is existing. For resonance frequencies, the acoustic cavity at the receiving side causes a decrease of the sound pressure in the receiving room.

The presence of the acoustic cavities also affects the velocity response of the panel. The velocity level difference results of the panel surface at the receiving side between the panel in the infinite baffle and niches for the three conditions are shown in Fig. 18.

The velocity responses of the panel for Conditions 1 and 3 are precisely the same, and so are those for Conditions 2 and 4. For off-resonance frequencies, the presence of the acoustic cavities increases the velocity response of the panel, and the difference at the off-resonance frequencies is generally less than 0. For resonance frequencies, the presence of the acoustic cavities decreases the velocity response of the panel, and the difference at the resonance frequencies is generally greater than 0.

To sum up, the STL results are influenced by the existence of the cavities on two sides. For off-resonance

frequencies, the presence of the acoustic cavities increases the velocity response of the panel, and the aperture at the receiving side increases the sound pressure in the receiving room. Thus, the STL results are decreased compared to the panel in the infinite rigid baffle. For resonance frequencies, the presence of the acoustic cavities decreases the velocity response of the panel, and the aperture at the receiving side decreases the sound pressure in the receiving room. Thus, the STL results are increased compared to the panel in the infinite rigid baffle.

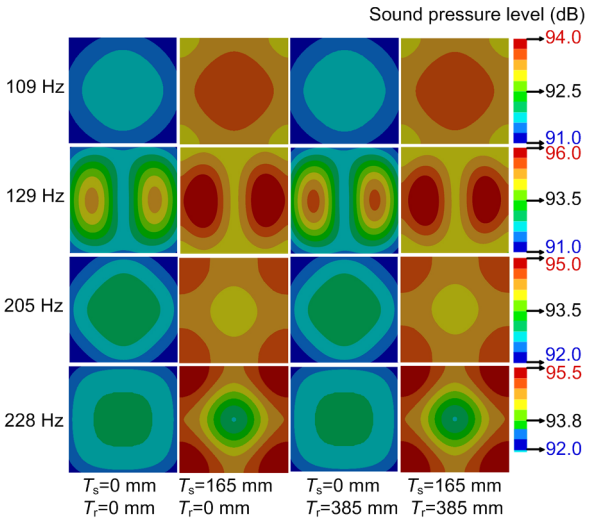

Fig. 16 Sound pressure level colour map for the panel surface closer to the source room

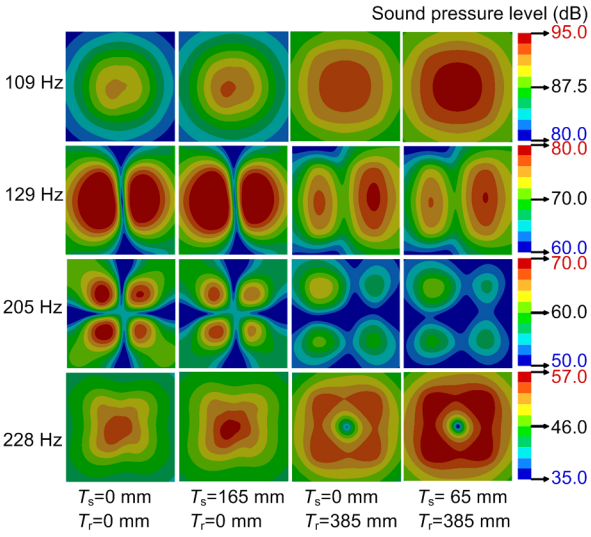

Fig. 17 Sound pressure level colour map of the AML surface of the receiving room

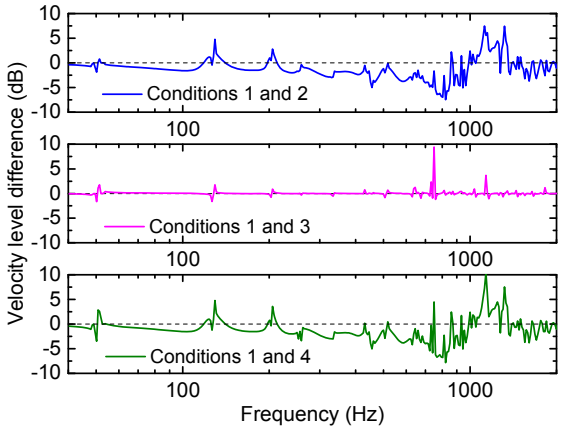

Fig. 18 Velocity level difference results of the panel surface at the receiving side

5.2 Effects of the mounting positions

The STLs for three different mounting positions mentioned in Table 1 are predicted. The boundary conditions of the panel are set as simply supported. The STL results for Conditions 4–6 for the 1/3 octave band and the discrete frequencies are shown in Figs. 19a and 19b, respectively.

Comparing the results for the three mounting positions under the simply supported boundary condition, in the 1/3 octave bands centred from 125 to 800 Hz, the STL decreases as the depth of the aperture in the source room increases from 0 to 165 mm. The maximum difference between 0 and 165 mm exceeds 5 dB. The difference at discrete frequencies is also large; the maximum standard deviation of the three conditions exceeds 4 dB.

5.3 Effects of the boundary conditions

5.3.1 Effects of two boundary constraints

Due to the influence of the test facility, the boundary constraints of the panel vary with different mounting positions. Two boundary conditions named ‘iron frame restraints’ and ‘four wooden blocks restraints’ are first considered. The mounting position of the panel is T_s=165 mm, T_r=385 mm. The results in the 1/3 octave band are shown in Fig. 20. The STL results at discrete frequencies for the two boundary conditions below 1000 Hz are shown in Fig. 21.

The STL results for the ‘iron frame restraints’ are smaller than for the ‘four wooden block restraints’ in the 1/3 octave bands centred from 100 to 125 Hz,

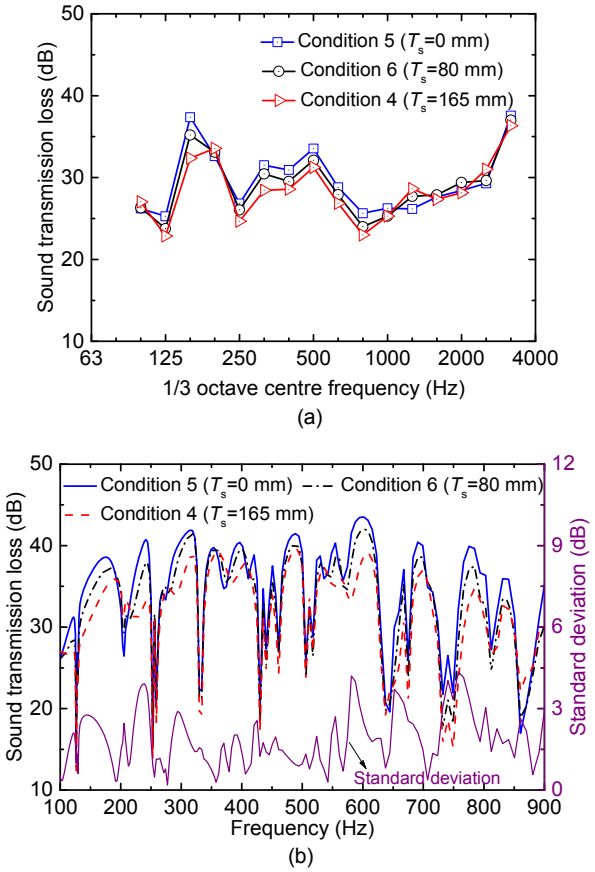

Fig. 19 STL predicted results of different mounting positions for the same boundary condition

(a) STL results for the 1/3 octave band; (b) STL results for the discrete frequencies

315 to 400 Hz, and 1000 to 1250 Hz when the panel is located in the niches. The STL results for the 'iron frame restraints' are larger than for the 'four wooden block restraints' in the 1/3 octave bands centred from 63 to 80 Hz and 500 to 800 Hz. The difference between the two boundary constraints is about 1.6 to 5.8 dB in the 1/3 octave bands centred from 125 to 1250 Hz. With the change in the boundary conditions from 'four wooden block restraints' to 'iron frame restraints', the STL valleys are shifted to higher frequencies, the natural frequencies are increased, and the range of the deviation between the two boundary conditions is increased.

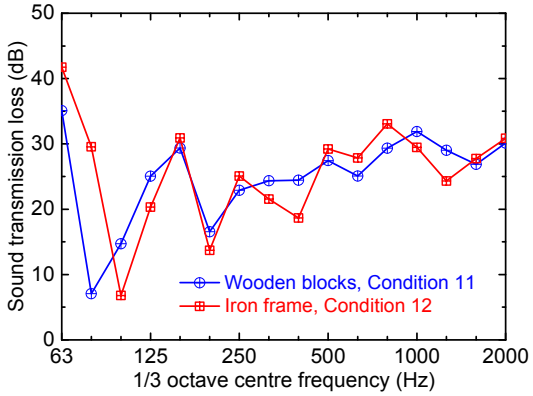

Fig. 20 Influence of the boundary constraints on the STL in the 1/3 octave band

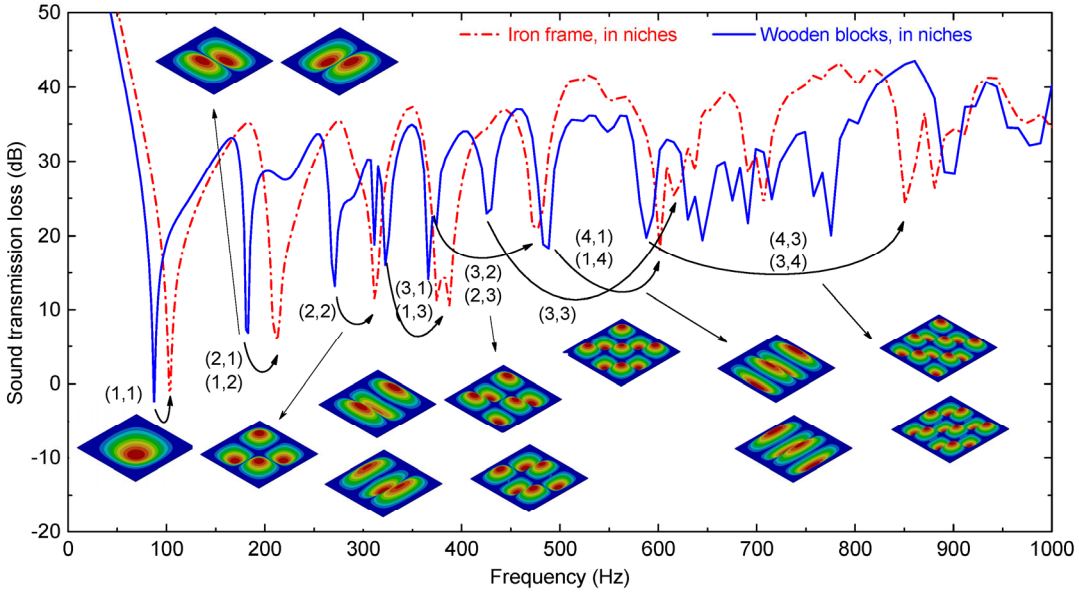

Fig. 21 Influence of the boundary constraints on the STL at discrete frequencies

The mounting position named 'baffled' (T_s= 0 mm, T_r=0 mm) is also considered to compare the influence of boundary constraints. The STL results for the 1/3 octave band and the discrete frequencies are shown in Figs. 22a and 22b, respectively.

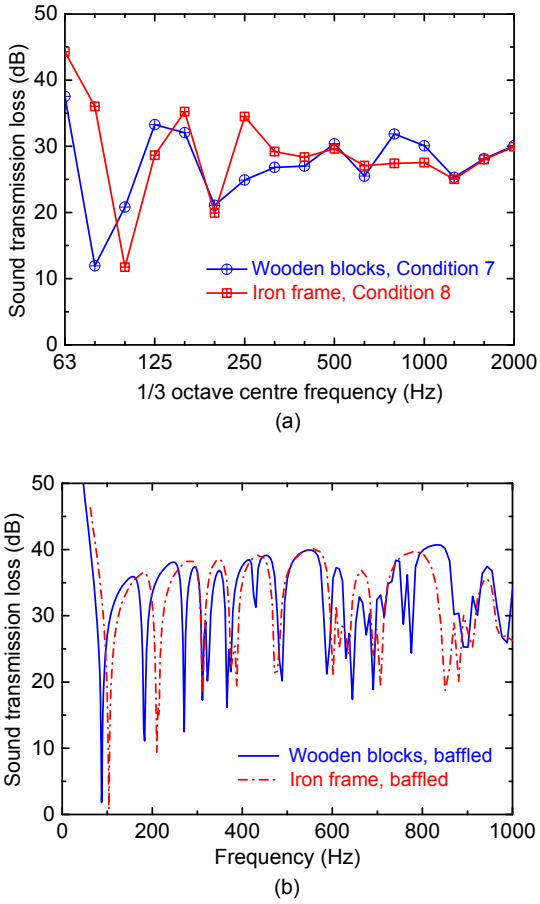

Fig. 22 STL predicted results of different boundary conditions when the panel is located in the infinite rigid baffle
(a) STL results for the 1/3 octave band; (b) STL results for the discrete frequencies

The STL results for the 'iron frame restraints' are smaller than for the 'four wooden block restraints' in the 1/3 octave bands centred from 100 to 125 Hz and 800 to 1000 Hz when the panel is located in the infinite rigid baffle. The STL results for the 'iron frame restraints' are larger than for the 'four wooden block restraints' in the 1/3 octave bands centred from 63 to 80 Hz and 250 to 315 Hz. The STL results for the two boundary constraints make small differences in the 1/3 octave bands centred from 400 to 630 Hz. The difference between the two boundary constraints is about 0.8 to 1.6 dB in the 1/3 octave bands centred from 400 to 630 Hz. With the change in the boundary conditions from 'four wooden block restraints' to 'iron frame restraints', the STL valleys are shifted to higher frequencies, leading to the STL differences between the two boundary conditions. Since the existence of the acoustic cavities can influence the STL results at resonance and off-resonance frequencies, the STL differences between the two conditions 'in niches' and 'baffled' become large because of the existence of the acoustic cavities, and the STL differences between the two boundary conditions are increased. The existence of the cavity amplifies the STL difference caused by the boundary conditions.

5.3.2 Effects of three typical boundary conditions

Three typical boundary conditions, including free, simply supported, and clamped, are considered. Two mounting positions named 'baffled' (T_s=0 mm, T_r=0 mm) and 'in niches' (T_s=165 mm, T_r=385 mm) are also compared to consider the influence of the niche effect. The standard deviations for the three boundary conditions of STL results are shown in Fig. 23.

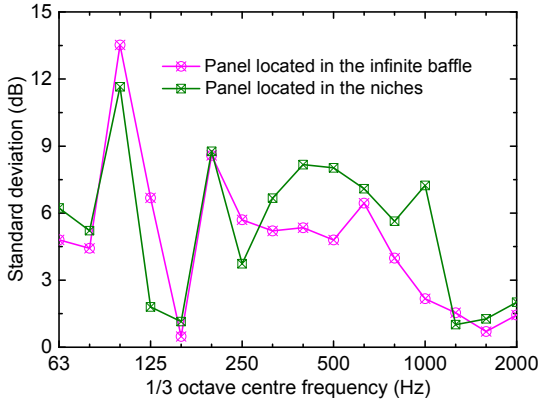

Fig. 23 Standard deviations for the three boundary conditions of STL results

The differences in the three boundary conditions are mainly concentrated in the 1/3 octave bands centred from 63 to 1000 Hz (below the coincidence frequency). The standard deviation for the three boundary conditions of STL results in the 1/3 octave bands centred from 315 to 1000 Hz is significantly larger

when the panel is located in the niches, compared to the standard deviation when the panel is located in the infinite baffle. The standard deviation for the three boundary conditions of STL results has a magnification larger than 1 dB at most frequencies.

The STL results for the three boundary conditions are shown in Fig. 24.

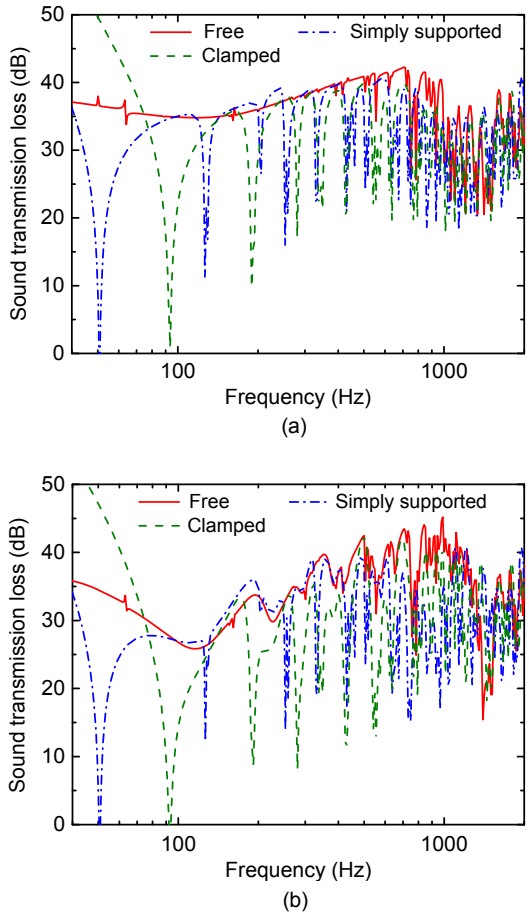

Fig. 24 Influence of typical boundary conditions on the STL results
(a) STL results for the baffled panel; (b) STL results for the panel in niches

There exist six rigid modes for free conditions, three for simply supported conditions, and none for the clamped condition. The presence of the rigid modes affects the STL results, especially in the low-frequency range below 125 Hz. As the boundary stiffness is increased, rigid modes in the free boundary condition gradually become constrained modes, and the natural frequencies of the modes are gradually increased. The STL valley starts to appear in the low-frequency domain, and the STL valley is moved to a higher frequency with the increase of boundary stiffness.

Comparing the STL results when the panel is located in the infinite baffle and the niches, the change of STL results at off-resonance frequencies becomes significant because of the existence of the acoustic cavities when the panel is located in the niches. The existence of the cavity amplifies the STL difference caused by the boundary conditions.

6 Conclusions

To investigate the influence of the mounting positions and the boundary conditions of lightweight panels on the STL results, the STLs of two typical lightweight panels in railway vehicles are tested, and a prediction model is established based on the finite element method. Combining the test and prediction results, it is found that during the STL measurements, the STL results can be strongly influenced by the mounting positions and the boundary conditions. Main findings of this study are summarised below:

1. For the two lightweight panels measured in this study, it is found that the STL results decrease when T_s (the depth of the aperture near the source room) increases from 0 to 165 mm (or 157 mm) at lower frequencies. However, at higher frequencies, STL is the greatest when T_s is 165 mm. The change of STL results during the measurement is entirely simulated by an STL prediction model based on the finite element method. STL results are affected by both the niches and the boundary conditions, and the impact of boundary conditions is larger at higher frequencies.

2. Considering the effects of mounting positions, the STL results are strongly influenced by the front and rear cavities. The difference between the panel in the infinite baffle and niches at the off-resonance frequencies is generally greater than 0, while the difference at resonance frequencies and the critical frequency is generally less than 0. For off-resonance frequencies, the presence of the acoustic cavities increases the velocity response of the panel, the aperture at the receiving side increases the sound pressure in the receiving room, and there is decreasing

STL compared to the panel in the infinite rigid baffle. For resonance frequencies, the acoustic cavities decrease the velocity response of the panel, and the aperture at the receiving side decreases the sound pressure in the receiving room, so the STL results are increased.

3. Considering the effects of boundary conditions, the STL results for the 'iron frame restraints' are larger than for the 'four wooden block restraints' in the 1/3 octave bands centred from 63 to 80 Hz and 500 to 800 Hz when the panel is located in the niches. With the change of boundary conditions, the STL valleys are shifted to higher frequencies, and the natural frequencies are increased. Then, the range of the deviation between the two boundary conditions is increased.

4. Considering both the effects of mounting positions and boundary conditions, the existence of the cavity amplifies the STL difference caused by the boundary conditions. When the panel is located in the niches, the STL difference results at resonance and off-resonance frequencies become significant because of the existence of the acoustic cavities, and the range of the deviation between the boundary conditions is increased compared to the STL difference when the panel is located in the infinite rigid baffle.

It is not easy to consider the real in situ mounting positions and mechanical boundary conditions of railway panel structures. In order to reduce the influence of mounting positions and mechanical boundary conditions on STL results, various mounting positions and mechanical boundary conditions are recommended during the measurement. The STL results should be averaged over multiple results.

Contributors

Dan YAO designed the research, finished the numerical simulations, and wrote the first draft of the manuscript. Jie ZHANG and Xin-biao XIAO helped to organize the manuscript. Rui-qian WANG finished the experiments. Dan YAO and Jie ZHANG revised and edited the final version.

Conflict of interest

Dan YAO, Jie ZHANG, Rui-qian WANG, and Xin-biao XIAO declare that they have no conflict of interest.

Acknowledgements

The authors would like to thank Yu-mei ZHANG and Ye LI (Southwest Jiaotong University, China) for their assistance in conducting the experiment, and Heng-yu WANG and Ji-ping DU (Southwest Jiaotong University, China) for their assistance in preparation of the manuscript.

References

Cremer L, 1942. Theorie der schalldämmung dünner wände bei schrägem einfall. *Akustische Zeitschrift*, 7(3):81-104 (in German).

Dai WQ, Zheng X, Luo L, et al., 2019. Prediction of high-speed train full-spectrum interior noise using statistical vibration and acoustic energy flow. *Applied Acoustics*, 145:205-219. https://doi.org/10.1016/j.apacoust.2018.10.010

de Langhe K, Moser C, Boeykens R, et al., 2016. Sound transmission loss predictions of aircraft panels: an update on recent technology evolutions. Proceedings of Inter-Noise and NOISE-CON Congress and Conference, p.6096-6107.

Dijckmans A, Vermeir G, 2012. A wave based model to predict the niche effect on sound transmission loss of single and double walls. *Acta Acustica United with Acustica*, 98(1):111-119. https://doi.org/10.3813/AAA.918497

Eade PW, Hardy AEJ, 1977. Railway vehicle internal noise. *Journal of Sound and Vibration*, 51(3):403-415. https://doi.org/10.1016/S0022-460X(77)80083-7

Fuller CR, Elliott SJ, Nelson PA, 1996. Active Control of Vibration. Elsevier, London, UK. https://doi.org/10.1016/B978-0-12-269440-0.X5000-6

Gholami MS, 2013. Vibro-acoustic Model to Predict Niche Effect on Sound Transmission Loss. MS Thesis, Universite de Sherbrooke, Canada.

ISO (International Organization for Standardization), 2000. Acoustics–Measurement of Sound Insulation in Buildings and of Building Elements Using Sound Intensity–Part 1: Laboratory Measurements, ISO 15186-1:2000. ISO, Geneva, Switzerland.

ISO (International Organization for Standardization), 2002. Acoustics–Measurement of Sound Insulation in Buildings and of Building Elements Using Sound Intensity–Part 3: Laboratory Measurements at Low Frequencies, ISO 15186-3:2002. ISO, Geneva, Switzerland.

ISO (International Organization for Standardization), 2010a. Acoustics–Laboratory Measurement of Sound Insulation of Building Elements–Part 1: Application Rules for Specific Products, ISO 10140-1:2010. ISO, Geneva, Switzerland.

ISO (International Organization for Standardization), 2010b. Acoustics–Laboratory Measurement of Sound Insulation of Building Elements–Part 2: Measurement of Airborne Sound Insulation, ISO 10140-2:2010. ISO, Geneva, Switzerland.

ISO (International Organization for Standardization), 2010c. Acoustics–Laboratory Measurement of Sound Insulation

of Building Elements–Part 4: Measurement Procedures and Requirements, ISO 10140-4:2010. ISO, Geneva, Switzerland.

ISO (International Organization for Standardization), 2010d. Acoustics–Laboratory Measurement of Sound Insulation of Building Elements–Part 5: Requirements for Test Facilities and Equipment, ISO 10140-5:2010. ISO, Geneva, Switzerland.

ISO (International Organization for Standardization), 2014. Acoustics–Determination and Application of Measurement Uncertainties in Building Acoustics–Part 1: Sound Insulation, ISO 12999-1:2014. ISO, Geneva, Switzerland.

Jin XS, 2014. Key problems faced in high-speed train operation. *Journal of Zhejiang University-SCIENCE A (Applied Physics & Engineering)*, 15(12):936-945. https://doi.org/10.1631/jzus.A1400338

Kihlman T, Nilsson AC, 1972. The effects of some laboratory designs and mounting conditions on reduction index measurements. *Journal of Sound and Vibration*, 24(3): 349-364. https://doi.org/10.1016/0022-460X(72)90749-3

Kim BK, Kang HJ, Kim JS, et al., 2004. Tunneling effect in sound transmission loss determination: theoretical approach. *The Journal of the Acoustical Society of America*, 115(5):2100-2109. https://doi.org/10.1121/1.1698815

Kim H, Ryue J, Thompson D, et al., 2016. Prediction of radiation ratio and sound transmission of complex extruded panel using wavenumber domain unite element and boundary element methods. *Journal of Physics: Conference Series*, 744(1):012144. https://doi.org/10.1088/1742-6596/744/1/012144

Kim K, Lee J, Kim D, 2012. A study on the vibroacoustic analysis of aluminum extrusion structures. *Computer-Aided Design and Applications*, 2:1-8. https://doi.org/10.3722/cadaps.2012.PACE.1-8

Kim TM, Kim JT, 2011. Comparison study of sound transmission loss in high speed train. *International Journal of Railway*, 4(1):19-27. https://doi.org/10.7782/IJR.2011.4.1.019

Liu XB, Yang Y, Le V, 2014. Airborne sound insulation of aluminum extrusion structural walls of an urban rail train. *Noise Control Engineering Journal*, 62(1):47-53. https://doi.org/10.3397/1/376205

Mao Q, Pietrzko S, 2013. Control of Noise and Structural Vibration: a MATLAB®-based Approach. Springer, London, UK. https://doi.org/10.1007/978-1-4471-5091-6

Schaffer H, Pucher E, 2013. Methods to simulate airborne sound transmission at railway door panels with deterministic wave theoretical approaches. *Journal of Materials Science and Engineering A*, 3(11):775-791.

Schroeder MR, 1996. The "Schroeder frequency" revisited. *The Journal of the Acoustical Society of America*, 99(5): 3240-3241. https://doi.org/10.1121/1.414868

Sgard F, Atalla N, Gholami M, et al., 2013. Tunneling effect on the sound transmission loss of a flat structure coupled with a porous material. *Proceedings of Meetings on Acoustics*, 19(1):065001. https://doi.org/10.1121/1.4798806

Sgard F, Atalla N, Nélisse H, 2015. Prediction of the niche effect for single flat panels with or without attached sound absorbing materials. *The Journal of the Acoustical Society of America*, 137(1):117-131. https://doi.org/10.1121/1.4901713

Thompson D, 2009. Railway Noise and Vibration. Elsevier, Oxford, UK. https://doi.org/10.1016/B978-0-08-045147-3.X0023-0

Utley WA, Fletcher BL, 1969. Influence of edge conditions on the sound insulation of windows. *Applied Acoustics*, 2(2):131-136. https://doi.org/10.1016/0003-682X(69)90015-2

Utley WA, Fletcher BL, 1973. The effect of edge conditions on the sound insulation of double windows. *Journal of Sound and Vibration*, 26(1):63-72. https://doi.org/10.1016/S0022-460X(73)80205-6

Vinokur R, 2006. Mechanism and calculation of the niche effect in airborne sound transmission. *The Journal of the Acoustical Society of America*, 119(4):2211-2219. https://doi.org/10.1121/1.2179656

Xie G, Thompson DJ, Jones CJC, 2006. A modelling approach for the vibroacoustic behaviour of aluminium extrusions used in railway vehicles. *Journal of Sound and Vibration*, 293(3-5):921-932. https://doi.org/10.1016/j.jsv.2005.12.015

Xin FX, Lu TJ, 2009. Analytical and experimental investigation on transmission loss of clamped double panels: implication of boundary effects. *The Journal of the Acoustical Society of America*, 125(3):1506-1517. https://doi.org/10.1121/1.3075766

Zhang J, Xiao XB, Sheng XZ, et al., 2016. SEA and contribution analysis for interior noise of a high speed train. *Applied Acoustics*, 112:158-170. https://doi.org/10.1016/j.apacoust.2016.05.019

中文概要

题　目：安装位置和边界条件对洞口中板件结构的隔声特性的影响

目　的：轨道列车车体结构的隔声性能对于控制轨道列车的内部噪声至关重要。在测试车体结构隔声特性时，声学实验室中存在很深的洞口，以便安装不同厚度的车体结构样件，并实现发声室和接收室的机械隔离。样件越小，安装位置和边界条件对

处在洞口中的板件结构的隔声特性的影响越大。本文旨在评估两种因素对结构隔声特性的影响，以解释真实结构的测试结果，并为实验室设计提供参考。

创新点： 1. 在实验室中测试了两种典型的轨道列车车体内地板结构在不同安装位置和不同边界条件下的隔声特性；2. 基于有限元法，建立了板件结构隔声特性预测模型，成功模拟了测试过程中的安装位置和边界条件，并对试验测试结果进行了再现和分析。

方　法： 1. 在实验室中，基于声压法测试两种内地板结构的隔声特性，并对比分析两种内地板结构在三种安装位置（两种边界条件）下的隔声特性（图 7 和 9）；2. 通过仿真模拟，基于有限元法建立内地板结构的隔声特性预测模型，并对模型进行验证（图 14）以及对试验测试结果进行再现（图 13）；3. 结合验证后的仿真预测模型，对比分析洞口（图 15~18）、位置（图 19）以及边界条件（图 20~24）对隔声特性的影响。

结　论： 1. 隔声测试结果受安装位置和边界条件共同影响，且边界条件在高频的影响更为显著；2. 如果单独考虑安装位置，那么受洞口中前后声腔的影响，隔声结果在共振频率和非共振频率的规律不同；3. 如果单独考虑边界条件，那么当边界条件发生变化时，隔声低谷会向高频或低频偏移，导致不同边界条件之间的隔声结果存在差异；4. 如果同时考虑安装位置和边界条件，那么洞口的存在会放大不同边界条件之间的隔声差异；5. 因为很难在实际测试中完全模拟轨道列车车体结构的安装位置和边界条件，所以在实验室测试时，建议选择几组不同的安装位置和边界条件，并对测试结果取平均值。

关键词： 隔声特性；轨道列车车体内地板；边界条件；安装位置；洞口效应